Synchronous polarization switching at sub-coercive fields through stochastic resonance in ferroelectric thin-film capacitors

Vivek Dey[1‖], Thejas Basavarajappa[1‖], Jonnalagadda Nikhila[2], …., Arvind Ajoy[2,], Pavan Nukala[1,*]*

[1]Centre for Nanoscience and Engineering, Indian Institute of Science, 560012, India

[2]Electrical Engineering, Indian Institute of Technology Palakkad, 678623, India

[‖] These authors contributed equally to this work

*Corresponding authors: pnukala@iisc.ac.in, arvindajoy@iitpkd.ac.in

Keywords: Stochastic resonance, non-volatile ferroelectric system, Landau model, Lead Zirconate, Frequency Shift Keying

Abstract

Stochastic resonance (SR) is a phenomenon by which the presence of noise in a non-linear system allows for detection of a weak sub-threshold signal, or in a bi-stable system allows for sub-threshold switching between the two states. Here we employ SR and demonstrate sub-coercive field synchronous switching with the drive waveform in a thin film ferroelectric lead zirconium titanate (PZT) capacitor. We further comprehensively model the device characteristics using stochastic time dependent Landau Ginzburg formulation and accurately simulate polarization switching and dynamics under application of noisy sub-coercive fields observed experimentally. We employ independent metrics such as cross-covariance, output power and signal-to-noise ratio to experimentally identify the optimal noise required for SR and show that these values are consistent with our device modeling. Finally, we show a proof-of-concept implementation of detecting sub-threshold frequency shift key signals in noisy communication channels using our ferroelectric PZT devices.

1. Introduction

Noise, in general, has a detrimental effect on systems performance as it introduces distortions in the signal under study. However, in a non-linear system, noise can counterintuitively

facilitate the retrieval of weak, sub-threshold signals. This phenomenon is facilitated by stochastic resonance (SR). Some of the first studies of SR and its mechanisms, were employed to explain long term climatic transitions and periodic recurrence of Earth's ice ages [1-4]. Since then, SR has been demonstrated in various systems, ranging from biological to physical systems [5-17]. For example, in sensory neurobiology, SR has been used to explain animal behaviors contributing to evolutionary success, such as the paddlefish, which uses optimal noise to efficiently detect its food, the zooplankton *Daphnia*, a task that would otherwise be impossible due to limited vision caused by poor light and turbid water [7,8]. SR demonstrations on electronic devices can be broadly classified as those on threshold devices, and those on nonvolatile devices (Fig. 1a). SR has been demonstrated in different thresholding devices such as Schmitt trigger circuits [9], tunnel diodes [10], bistable ring laser [11], MoS_2 photodetectors [12], metal-oxide memristive devices [13] and many others [14-17]. However, modeling approaches to understand the physics of SR in these devices are lacking.

There are very limited studies pertaining to SR in non-volatile systems. Ferroelectric devices, with their characteristic double-well potential, represent a classic example of non-volatile bistable systems. In these systems, at sub-coercive fields, noise dictates the rate at which the system jumps from one well to another (Kramers rate, r_k). The noise (optimal) when $r_k = 2r_s$, where ω_s ($=2\pi r_s$) is the drive frequency, defines the condition for SR. SR has been studied in TGS single crystals [18] but the ferroelectric nature of the material remains unclear due to the weak ferroelectricity, making it difficult to distinguish dielectric hysteresis from ferroelectric polarization. In our study, we utilize thin-film PZT devices, well-established and robust ferroelectric material system, to demonstrate stochastic resonance (SR) at sub-coercive voltages (0.75 V_c). We quantify the optimal noise for SR at $0.75V_c$ through four independent figures of merits: cross-covariance, output power, signal-to-noise ratio1 and signal-to-noise ratio 2. We model the bistable non-volatility of our devices through Landau theory, and employ stochastic time dependent Ginzburg Landau (TDGL) formulation to simulate

polarization switching and dynamics at sub-coercive voltages under the presence of noise. We derive the figures of merit, which accurately match with the experimental data. Our modeling and experiments provide deep insights into dynamics of SR through the phenomenological parameters of the bi-stable (double well) system. Finally, we present a proof-of-concept implementation of sub-threshold frequency shift key signal recovery using SR in our devices. This highlights the potential of our approach for enhancing signal detection in noisy communication channels, such as underwater communication.

2. PZT thin film ferroelectric device characterization and modeling through TDGL

We use PZT thin film capacitors (255 *nm*) sandwiched between TiO_2(40 *nm*)/Pt (150 *nm*) as bottom electrode and Pt (thickness = 100 *nm*, area = 4000 μm^2) as top electrode hosted on thermally oxidized silicon substrate. Fig 1b shows the polarization vs electric field (PE) hysteresis plot obtained from the PUND measurement on our device, with coercive voltage (V_c) and remnant polarization (P_r) extracted to be 2.1 V and 17 $\mu C/cm^2$, respectively.

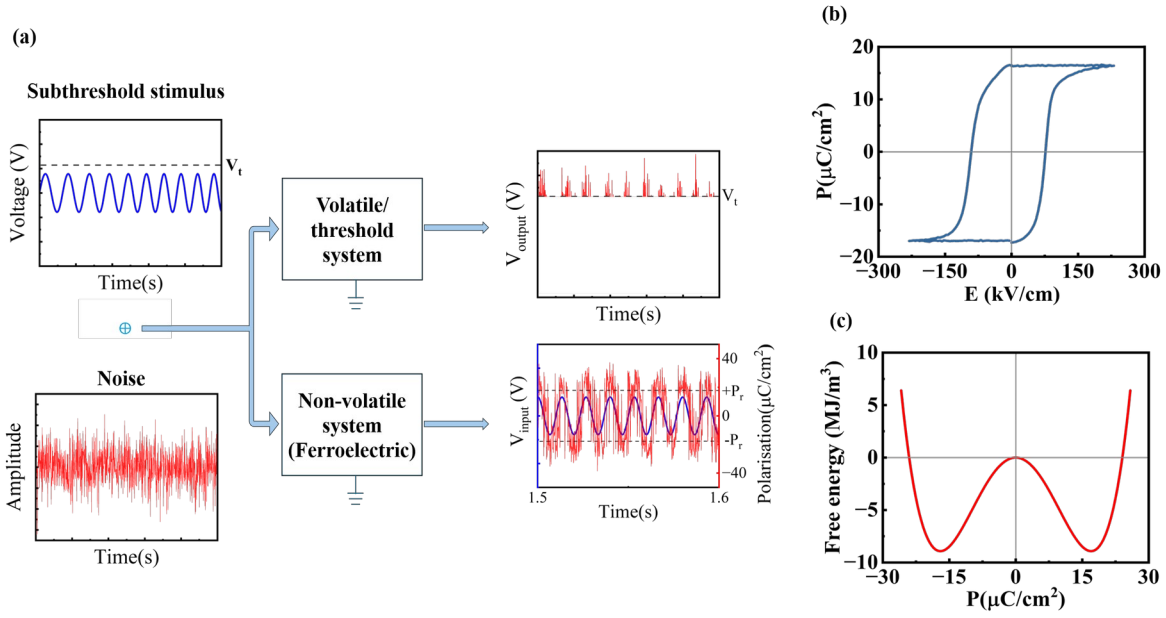

Fig 1. Concept of SR and PZT device characterization. (a) Schematic of the stochastic resonance in a volatile/threshold and non-volatile bistable systems. (b) Polarization vs electric field hysteresis loop measured for our PZT device of area 4000 μm^2. (c) Free energy vs

polarization plot representing the bistable potential well of the PZT device modeled using Landau theory at zero bias.

We model the ferroelectric bistable potential well using Landau free energy density as,

$$F = \alpha P^2 + \beta P^4 - P.E \qquad (1)$$

here, α = $-3\sqrt{3}E_c/4P_r$ and $\beta = 3\sqrt{3}E_c/8P_r^3$ are the Landau coefficients [19] and E is the applied electric field. For our devices, the value of P_r = 17 $\mu C/cm^2$ and E_c = 83.6 kV/cm and hence estimated α = 6.34×10^9 cmF^{-1} and β = 1.09×10^{15} cm^5 $F^{-1}C^{-2}$. From these parameters we can extract a symmetrical double well potential for our device with a barrier height of ΔF = 0.9×10^6 Jm^{-3}, shown in Fig 1c.

The dynamics of polarization with white gaussian noise ($\xi(t)$) can be understood by solving the following stochastic time dependent Ginzburg-Landau equation (TDGL) [20],

$$\rho \frac{\partial P}{\partial t} = \frac{-\partial F}{\partial P} + \xi(t) \qquad (2)$$

The polarization is thus a stochastic variable, with a diffusion coefficient "D" arising from an underlying Brownian motion or Weiner process ($W(t)$), related to $\xi(t)$ as,

$$\xi(t) = \sqrt{2\rho D}\frac{dW(t)}{dt} \qquad (3)$$

where ρ is the switching resistivity of the device, a dissipative term. A more rigorous formulation can be found in [20-25] (also explained in Supplementary Note 1). The Gaussian noise, and hence the D coefficient has two independent sources: internal (thermal, $D_{\int} = \frac{k_B T}{t_F A_F}$), and external ($D_{ext}$) sources. In the simulations that follow, ignoring internal noise (D_{int}), D_{ext} can be expressed as , $D_{ext} = \frac{V_{rms}^2}{2\rho\Delta f t_f^2}$,[20] where, k_B is Boltzmann's constant, T is temperature of the system, V_{rms} is the root mean squared value of the external noise, Δf is the bandwidth of the external noise, t_F is thickness of the PZT thin film. Following ref [20], we express the standard deviation of the Gaussian noise in a scaled form as $D_{ext}/\Delta F$.

To estimate ρ we reconfigure the TDGL equation as having capacitive and resistive contribution and construct an equivalent RC circuit as shown in Fig S2. Following the procedure described in Supplementary Note 2, the value of ρ is calculated to be 1367.16 Ωm from the derived expression $E_c = \rho \frac{I_c}{A}$, where the I_c is the current through the equivalent resistor at P = 0 i.e., the switching current.

Equation 2 can now be rewritten in a discretized form as the following:

$$P[i] = P[i-1] - \frac{\Delta t}{\rho} . \frac{\partial F}{\partial P}[i-1] + \sqrt{\frac{2 D_{ext}}{\rho}} . \Delta w[i-1] \qquad (4)$$

where $[i]$ represents the i^{th} timestep, Δt is the simulation timestep and $\Delta w[i]$, which is the increment in the random noise at every simulation timestep is extracted from a normal distribution with mean 0 and variance Δt. This was solved using the Euler-Maruyama method [26] to obtain the temporal change of polarization under the application of weak sub-threshold signal.

Fig 2 (and Fig S2) shows the simulated polarization vs time plots at different noise strengths, $D_{ext}/\Delta F$ for 75 *Hz*, (100 and 150 *Hz*) signals at a sub-coercive voltage of 0.75 V_c. For 75 *Hz* signal, we note that at $D_{ext}/\Delta F$ = 0.06 the polarization does not switch, and at $D_{ext}/\Delta F$ = 6.19, the polarization switches randomly and asynchronously with the drive voltage signal. However, at a $D_{ext}/\Delta F$ = 0.87, a value in between, the polarization switches quasi-periodically in response to the input sub-coercive voltage, indicating stochastic resonance.

To rigorously characterize SR, we introduce the following figures of merit:

(a) Cross-covariance: Cross-covariance is calculated between the reference polarization signal ($P_1(t)$) obtained from a sinusoidal input voltage signal without external noise with V_{max} = 2*V_c, and the observed polarization signal ($P_2(t)$) at sub-threshold voltages with noise.

$$cov(V_1, V_2) = \frac{1}{N-1} \sum_{i=1}^{N} (P_1 - \mu_1) * (P_2 - \mu_2) \qquad (5)$$

where N is the number of samples in the voltage signal and $\mu_1$and μ_2 are the average values of the two signals P_1 and P_2.

(b) Output power: The total power within the carrier frequency band defined by (Δf = 8 *Hz*) output polarization signal is calculated as

$$OP = \int_{f_1}^{f_2} (PSD)\, df$$

(c) Signal to noise ratio-1 (SNR_1): SNR_1 is obtained as ratio of peak power of the signal at the drive frequency (f_s, Δf_s), and noise power within a selected frequency range. For f_s = 75, 100 and 150 *Hz*, Δf = 60 *Hz* and background noise interval (f_1 and f_2) are 15 and 135 *Hz*), 40 and 160 *Hz*, 90 and 210 respectively.

(d) Signal to noise ratio-2 (*SNR-2*):

For the double well potential of our PZT devices, we find that all the independent figures of merit *cov*, *OP* and SNR_1 peak at $D_{ext}/\Delta F$ = 0.87 ± 0.15, which is the optimal noise for SR as estimated from our numerical analysis.

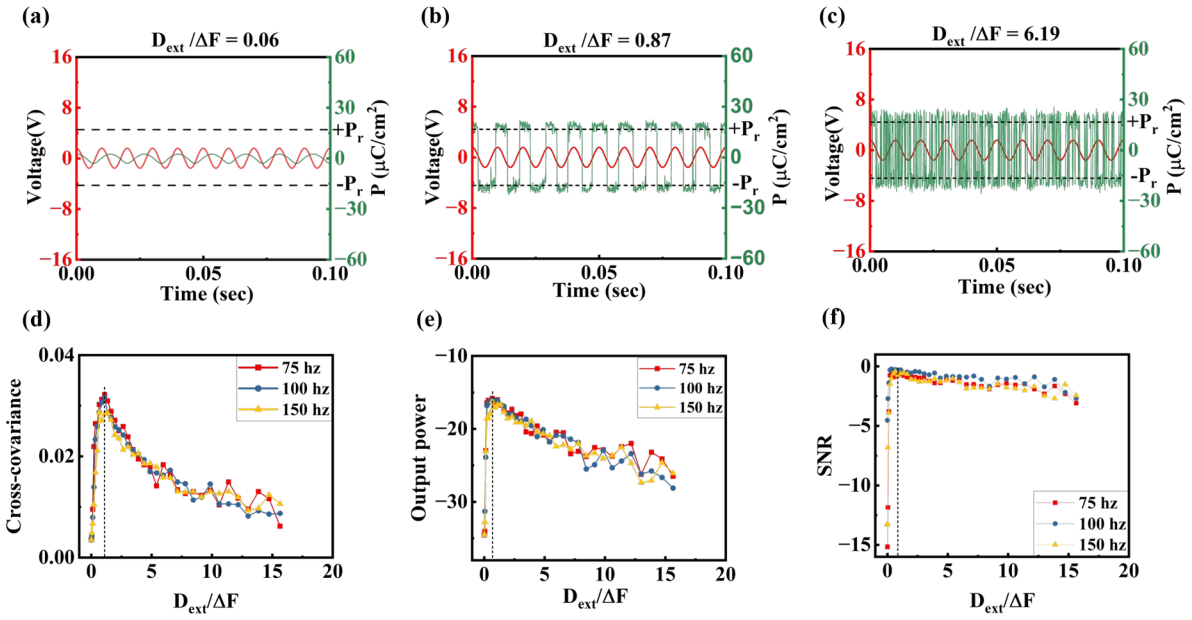

Fig 2. SR simulation. (a)-(c) Polarization vs time recordings with input signal with amplitude 0.75 V_c and 75 *Hz* as signal frequency for different $D_{ext}/\Delta F$. Different metrics quantifying

stochastic resonance (d) cross-covariance, (e) output power, and (f) output snr. The optimum $D_{ext}/\Delta F$ at which SR occurs is shown in vertical black dotted lines.

3. Experimental demonstration of stochastic resonance

Next, we apply sub-coercive voltage signals to the PZT device in the presence of noise and record the polarization switching. For this, we generate sub-coercive periodic voltage signals of an amplitude of 0.75 V_c at different frequencies 75 *Hz*, 100 *Hz* and 150 *Hz* feed it into the device by adding white gaussian noise of bandwidth 10 *kHz* with mean 0 and varying standard deviation (σ) (see methods and Supplementary Note 3). The devices are poled before every cycle of measurements to ensure that the starting state is the same well in the double well potential (for poling protocols, see Supplementary Note 4). Fig. 3 (Fig S3) shows P vs t response for 75 *Hz* (100, 150 *Hz*) at different noise strengths, $D_{ext}/\Delta F$. P_r and $-P_r$ values obtained from the PE loop (Fig 1b) are shown as dotted lines, and any polarization switching event will involve change in polarization $P < -P_r$ to $P > P_r$ or vice versa. Changes in polarization within these limits are just a result of dielectric charging and not polarization switching. Using these identification markers, we clearly see that quasi periodic switching occurs at an optimal value of noise (Fig 3b, $D_{ext}/\Delta F = 0.87$), with large noise (Fig 3c, $D_{ext}/\Delta F = 6.19$) asynchronously switching the device, and small noise just leading to dielectric charging (Fig 3a, $D_{ext}/\Delta F = 0.06$).

We further estimate the figures of merit (*cov*, *OP*, SNR_1) and show that they peak at an optimal value of noise, corresponding to SR. Upon comparing all the independent figures of merit estimated from experimental data with those obtained from stochastic TDGL simulations, we find an accurate match between the two, emphasizing the robustness of our phenomenological modeling framework (Fig 3g-i). Note that in the DUT, $D_{ext}/\Delta F \sim 0.87$ is the optimal noise required for SR in the tested frequency regimes.

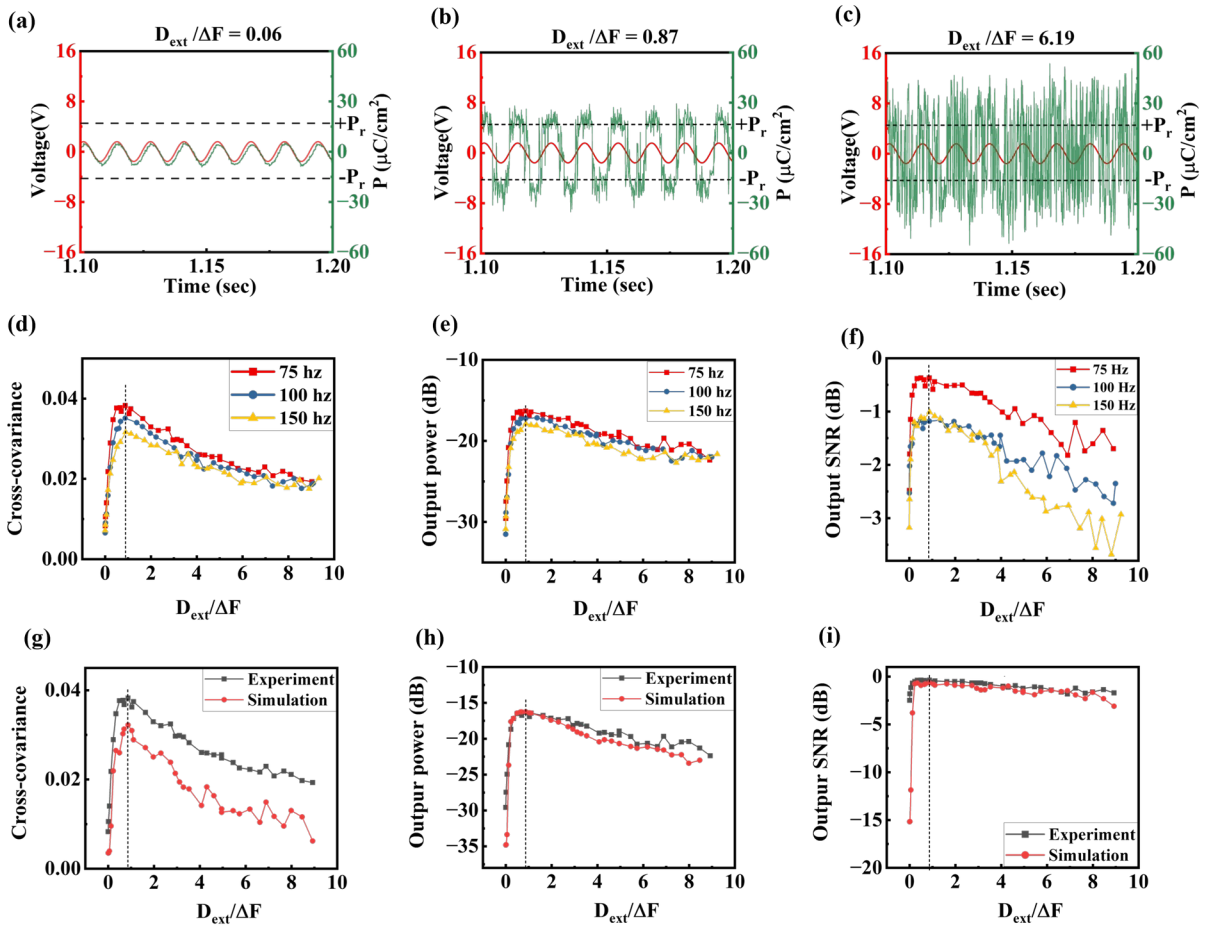

Fig 3. SR experiment. (a)-(c) Simulated Polarization vs time recordings with input signal as 0.75 V_c and 75 *Hz* as signal frequency for different $D_{ext}/\Delta F$. Different metrics quantifying stochastic resonance (SR) (d) cross-covariance, (e) output power, and (f) output snr (SNR_1). The optimum $D_{ext}/\Delta F$ at which SR occurs is shown in vertical black dotted lines. (g), (h) and (i) are comparisons of simulation and experimental results of different metrics at 75 *Hz* input signal. Both experiment and simulation shows SR peaks at similar value of $D_{ext}/\Delta F \sim 0.87$.

4. Detection of sub-threshold frequency shift key signals in noisy environments:

Frequency-Shift Keying (FSK) is a method of digital signal modulation where binary or multibit data is encoded in the frequency of a carrier signal and transmitted across a communication channel. FSK is widely used in applications such as radio communication, modems, and other wireless communication systems [27-29]. However, the recovery of such signals in a noisy environment is challenging due to energy loss during transmission through

these channels. Here, we show that SR in a ferroelectric bistable system can be a promising receiver unit that can detect and recover the weak subthreshold FSK signal.

In Fig 4, we show an example of a frequency encoded message in a binary signal *m(t)* of bitrate 5 bit/s (Fig. 4a), with bits 0 and 1 corresponding to f_0: 37 Hz and f_1: 75 Hz respectively. Then the instantaneous frequency, $f_m(t)$, of the transmitted FSK signal is determined by the binary modulating signal, *m(t)* as,

$$f_m(t) = f_0 + (f_0 - f_1).m(t) \qquad (6)$$

Then the FSK signal through the channel can be written as,

$$V_{signal} = V_0 \sin\left(2\pi \sum_{i=0}^{n} f_m(t_i).\Delta t\right) \qquad (7)$$

where V_0 is the amplitude of the carrier signal and Δt is the sampling time interval (Fig 4b). This signal gets damped upon transmission in a channel, and the challenge hence is to recover the frequency components at the receiver. To this end, we fed the sub-threshold FSK signal modulated with white Gaussian noise to the receiver which is our ferroelectric PZT device.

$$V_{device} = V_{signal} + noise \qquad (8)$$

The ensuing polarization response is measured, and at optimal noise corresponding to SR ($D_{ext}/\Delta F \sim 0.87$), the frequency information of the sub-threshold signal is transferred with maximum fidelity (Fig 4c). In the example considered, the demodulated signal (see methods) is 100% recovered (Fig 4d), showing a proof-of-concept that the idea of SR in ferroelectric devices can be exploited for efficient signal recovery.

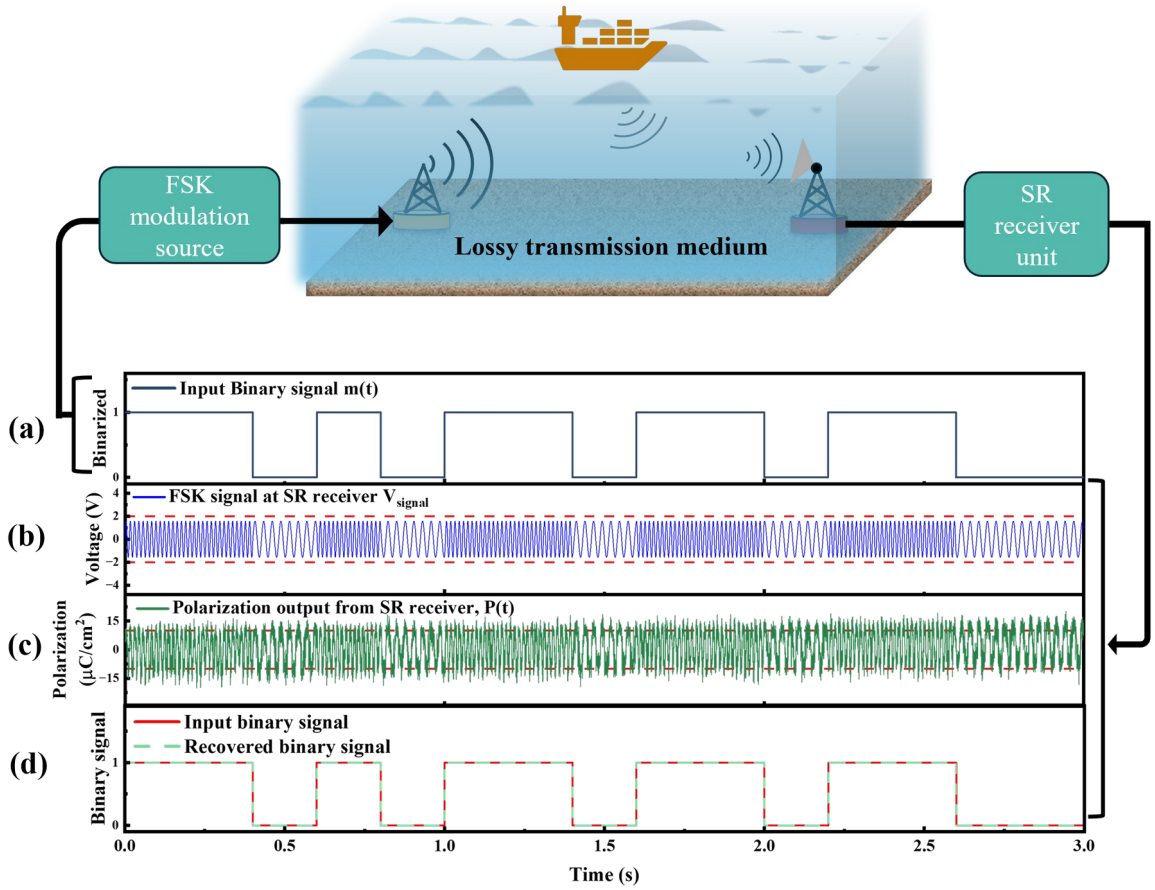

Fig 4. B-FSK signal recovery. Top: Schematic of underwater communication where the information encoded as FSK signal transmitted through a lossy medium gets distorted. (a) Binary signal m(t) (bitrate 5bit/s) containing message that needs to be transmitted. (b) The distorted (sub-coercive) FSK signal after travelling through the noisy channel (modulated with frequencies f_0: 37 Hz and f_1: 75 Hz corresponding to the information encoded in bits 0 and 1 respectively). (c) The polarization output of the SR receiver in response to the distorted FSK signal alongwith optimal noise. (d) Recovered binary signal through the method of temporal dominant frequency contents in polarization output.

5. Conclusions

In this study, we demonstrate stochastic resonance (SR) in a bistable ferroelectric potential well by modulating the well with a weak sub-threshold periodic signal in the presence of noise. We show that at an optimal noise strength, the polarization state of PZT switches quasi-periodically in synchronization with the input signal frequency. We model the bistable

potential well of PZT based on Landau theory and simulate the polarization dynamics by solving the stochastic time-dependent Ginzburg-Landau (TDGL) equation using the Euler-Maruyama method. SR is observed at an optimal noise strength, which accurately matches the experimental observations. Finally, we explore the application of SR in frequency shift keying (FSK) signal recovery, demonstrating that ferroelectric SR can serve as a robust recovery mechanism due to its ability to detect sub-threshold signals with great fidelity in noisy environments.

Methods

Material:

Lead zirconium titanate (PZT) capacitor samples (purchased from Radiant Technologies) are used for the study of SR. The PZT device has the stacking of SiO_2(500nm)/TiO_2(40nm)/Pt(150nm)/PZT (255nm)/Pt(100nm) with the top electrode area = 4000 μm^2.

Electrical measurements: The electrical measurements are performed in a probe station of Multi System Analyzer 500 using Precision Multiferroic II Ferroelectric Tester. Before every measurement, i.e., feeding sub-coercive signal + noise to PZT device, we pole the sample by applying two opposite poling pulses with amplitude > V_c in order to start with the same reference P_r values and V_c. More detailed measurement protocols are discussed in detail in Supplementary.

Data analysis: The numerical simulations of Landau theory for our PZT device and the output polarization recordings of experiment and simulation are analyzed using in-house developed code in MATLAB. The functions *cov,* bandpower, and pwelch in MATLAB are used to estimate cross-covariance, output power, and PSD for SNR-1 respectively.

Acknowledgements

P.N. acknowledges Start-up grant from IISc, Infosys Young Researcher award, and SERB (DST), New Delhi, Govt. of India CRG/2022/003506. PN and VD acknowledge the usage of national nanofabrication center, micro nano characterization center, and advanced facility for microscopy and microanalysis of IISc for various fabrication and characterization studies.

References

1. Benzi, R., Sutera, A. & Vulpiani, A. The mechanism of stochastic resonance. J. Phys. A: Math. Gen. 14, L453 (1981).
2. Benzi, R., Parisi, G., Sutera, A. & Vulpiani, A. Stochastic resonance in climatic change. Tellus 34, 10 (1982).
3. Nicolis, C. Stochastic aspects of climatic transitions - response to a periodic forcing. Tellus 34, 1 (1982).
4. Nicolis, C. Long-term climatic transitions and stochastic resonance. J. Stat. Phys. 70, 3–14 (1993).
5. Douglass, J. K., Wilkens, L., Pantazelou, E. & Moss, F. Noise enhancement of information transfer in crayfish mechanoreceptors by stochastic resonance. Nature 365, 337 (1993).
6. Levin, J. E. & Miller, J. P. Broadband neural encoding in the cricket cereal sensory system enhanced by stochastic resonance. Nature 380, 165 (1996).
7. Russell, D. F., Wilkens, L. A. & Moss, F. Use of behavioural stochastic resonance by paddle fish for feeding. Nature 402, 291 (1999).
8. Freund, J. A. et al. Behavioral stochastic resonance: how the noise from a Daphnia swarm enhances individual prey capture by juvenile paddlefish. J. Theor. Biol. 214, 71–83 (2002).
9. Fauve, S. & Heslot, F. Stochastic resonance in a bistable system. Phys. Lett. A 97, 5–7 (1983).
10. Mantegna, R. N. & Spagnolo, B. Stochastic resonance in a tunnel diode. Phys. Rev. E 49, R1792–R1795 (1994).
11. McNamara, B., Wiesenfeld, K. & Roy, R. Observation of stochastic resonance in a ring laser. Phys. Rev. Lett. 60, 2626 (1988).
12. Dodda, A., Oberoi, A., Sebastian, A., Choudhury, T. H., Redwing, J. M. & Das, S. Stochastic resonance in MoS_2 photodetector. Nat. Commun. 11, 4406 (2020).

13. Mikhaylov, A. N., et al. Stochastic resonance in a metal-oxide memristive device. Chaos Solitons Fractals 144, 110723 (2021).
14. Hakamata, Y., Ohno, Y., Maehashi, K., Inoue, K. & Matsumoto, K. Robust noise characteristics in carbon nanotube transistors based on stochastic resonance and their summing networks. Jpn. J. Appl. Phys. 50, 06GE03 (2011).
15. Hibbs, A., et al. Stochastic resonance in a superconducting loop with a Josephson junction. J. Appl. Phys. 77, 2582–2590 (1995).
16. Dykman, M., et al. Noise-enhanced optical heterodyning in an all-optical bistable system. Appl. Phys. Lett. 67, 308–310 (1995).
17. Gammaitoni, L., Martinelli, M., Pardi, L. & Santucci, S. Observation of stochastic resonance in bistable electron-paramagnetic-resonance systems. Phys. Rev. Lett. 67, 1799 (1991).
18. Diestelhorst, M. & Drozhdin, K. Stochastic resonance in ferroelectric Triglycine sulfate. Ferroelectrics 238, 25–32 (2000).
19. Lin, C.-I., Khan, A. I., Salahuddin, S. & Hu, C. Effects of the Variation of Ferroelectric Properties on Negative Capacitance FET Characteristics. IEEE Trans. Electron Devices 63, 2197–2199 (2016).
20. Ramesh, M., Verma, A. & Ajoy, A. Kramers' escape problem for white noise driven switching in ferroelectrics. arXiv Preprint 2112.01373 (2022). https://arxiv.org/abs/2112.01373.
21. Nambu, S. & Sagala, D. A. Domain formation and elastic long-range interaction in ferroelectric perovskites. Phys. Rev. B 50, 5838–5847 (1994).
22. Levy, B. Wiener Process and White Gaussian Noise. pp. 207–234 (2020).
23. Liyanagedera, C. M., Sengupta, A., Jaiswal, A. & Roy, K. Stochastic spiking neural networks enabled by magnetic tunnel junctions: From nontelegraphic to telegraphic switching regimes. *Phys. Rev. Appl.* **8**, 064017 (2017).
24. Etesami, S., Sukhov, A. & Berakdar, J. Kinetics of nanosize ferroelectrics. Phys. Rev. B 94, 174105 (2016).
25. Risken, H. The Fokker-Planck Equation: Methods of Solution and Applications (Springer, Berlin, 1996).
26. Platen, E. An introduction to numerical methods for stochastic differential equations. Acta Numerica 8, 197–246 (1999).